Title
CLIMB OF DISLOCATIONS IN MAGNESIUM OXIDE SINGLE CRYSTALS

Author
Narayan, Jagdish.

Publication Date
1970-09-01

UCRL-20305 c. 2

CLIMB OF DISLOCATIONS IN MAGNESIUM OXIDE SINGLE CRYSTALS

Jagdish Narayan
(M. S. Thesis)

September 1970

AEC Contract No. W-7405-eng-48

LAWRENCE RADIATION LABORATORY
UNIVERSITY of CALIFORNIA BERKELEY

UCRL-20305 c. 2

25

DISCLAIMER

Contents

CLIMB OF DISLOCATIONS IN MAGNESIUM OXIDE SINGLE CRYSTALS

Jagdish Narayan

Inorganic Materials Research Division, Lawrence Radiation Laboratory
Department of Materials Science and Engineering, College of Engineering
University of California, Berkeley, California

ABSTRACT

The wave like pattern, observed in dislocation dipoles* of uniform spacing during annealing, which starts from the ends of the dipole and gets damped toward the centre, has been attributed to controlled vacancy migration.** A theory has been set-up to give activation energy for the process, 60,700 ± 2,000 cal/mole. This value has been compared with an independent study of pipe diffusion,† in which a prismatic loop inside the foil is connected to both surfaces of the foil by another screw dislocation.

A theory set-up for the latter gives the diffusion equation:

$$D_p = 1.5 \times 10^{-3} \exp(-60{,}400/RT)$$

and the value of entropy $\Delta S = 0.1$ cal/mole·deg.

In the diffusion process, both oxygen and magnesium ions take part, but the rate is controlled by oxygen ion mobility.

---

*Two dislocations of opposite signs and closely spaced.

**Diffusion, along the dislocation, is limited within one wavelength.

†Diffusion along the core of a dislocation.

I. INTRODUCTION

Earlier transmission electron microscopic studies on magnesium oxide, deformed plastically either by bending or compression, have provided information concerning the nature of the dislocation distribution,[1,2] the mechanism of dipole formation,[3,4,5] the kinetics of breaking of dipoles and subsequent annealing behavior.[6,7] However questions still remain concerning the following.

(i) The mechanism of termination of dipoles

(ii) The mechanism of dipole break-up into rows of prismatic loops and a precise value for the activation energy of this process; the extra stability of dumbell shaped dipoles, during annealing.

(iii) Direct evidence of pipe diffusion and its activation energy is still lacking.

(iv) The mechanism of climb of dislocation loops during annealing after complete break-up of dipoles and the activation energy of the bulk diffusion process involved are still uncertain.

(v) Prismatic slip and conservative climb of dislocation loops due to annealing.

(vi) The nature of dislocation loops formed between slip bands during annealing.

Experiments have been done which give further information concerning all of these questions, but this report will be limited to (ii) and (iii).

The plastic deformation of magnesium oxide single crystals produces slip bands corresponding to $\{110\}\langle 1\bar{1}0\rangle$ slip. These slip bands consist of

dislocation dipoles as well as individual screw and edge dislocations. Slip bands contain dipoles of all sizes and nature and dislocations from pure edge to pure screw. However most of the damage is in the form of dipoles.

The kinetics of breaking of these dipoles into prismatic loops on annealing, studied by Groves and Kelly[6] gives only an upper limit of the activation energy for pipe diffusion. Also, since the spacing of the dipoles studied by them was unresolvable in the electron microscope, the mechanism of dipole breaking was not understood clearly.

By developing a technique of annealing electron microscope foils outside the microscope and observing the same area repeatedly, we have studied the annealing kinetics of dipoles whose spacing is clearly resolvable. This not only reveals the mechanism of dipole breaking, but also a better value of the activation energy for pipe diffusion has been estimated by measuring the change in amplitude after each annealing treatment.

Another way to study the pipe diffusion process is to find a configuration where either a vacancy or an interstitial loop inside the foil is connected to surfaces of the foil by another dislocation and then measure the shrinkage rate, during a series of annealing treatments outside the electron microscope. From this we can estimate the activation energy for the pipe diffusion on the basis of a simple diffusion equation. This provides direct evidence of pipe diffusion. Also, the value of the activation energy and kinetics are more reliable than any obtained in the past.

II. EXPERIMENTAL PROCEDURE

A. Material

Magnesium oxide supplied by Muscle Shoals Electrochemical Corp., Tuscumbia, Alabama was used for the experiments. The following are the impurities reported by American Spectrographic Laboratories.

Al - .06%, Fe - .03%
Ca - .03%, Mn - .002%
Cr - .002%, Cu - < .001%
Si - < .005%

B. Specimen Preparation

Material, as supplied, was polycrystalline of very large grain size. Single crystal specimens in the form of thin sheets (~0.50 ~ 0.25 mm thick) were obtained by cleaving carefully along (100) crystallographic planes. The surface damage introduced during cleaving was removed and subsequently the sheets were thinned down to ~0.1 mm by chemical polishing in hot phosphoric acid (150 - 160°C). These samples were bent backwards and forwards (±5 cm radius) about 200 times till they were full of slip bands all over. Then the samples were thinned down further, after applying masking lacquer around the edges, by chemically polishing in hot phosphoric acid. Final thinning to get electron microscope samples was done by a jet polishing technique.[1] After cold working the thinning was done from one side as far as possible because damage is maximum at the surfaces and minimum at the centre.

C. Foil Orientation and Electron Microscopy

When a thin sheet is bent along [010] axis, dipoles are introduced on (101) $[\bar{1}01]$, $(\bar{1}01)$ [101] and on (110) $[\bar{1}10]$, $(\bar{1}10)$ [110] slip systems

as shown in Fig. 1.

Dipoles on (101)[$\bar{1}$01] and ($\bar{1}$01) [101] are of primary interest as dipoles on (110) [$\bar{1}$10] and ($\bar{1}$10) [110] are seen edge on. If the bending axis is slightly off from [010], dipoles on (011) [0$\bar{1}$1] and (0$\bar{1}$1)[011] also appear.

The foil surface is perpendicular to the [001] direction. For the electron microscope the 200 reflection was used because this makes sure that observed dipoles lie on (101) planes, not on (011) planes. The latter might occassionally be present.

All the foils were examined in a Siemens 100 kV electron microscope. A double tilt holder was used. The same area was observed repeatedly after annealing at constant temperature outside the electron microscope and cooling in air.

III. THEORIES

A. Model for Breaking of Dipoles

The following derivation is based on the assumption that the dipole is infinitely long, breaking occurs far away from both ends and on experimentally observed fact that diffusion is of a very localized nature.

Referring to Fig. 2 let the fluctuation be represented by

$$y = h + a \sin px \tag{1}$$

There is a force F per unit length, acting on the dislocation due to other dislocation of the dipole, which makes it climb. The concentration of vacancies C in the vicinity of the dislocation is given by

$$C = Co \exp Fb^2/RT \tag{2}$$

where Co is the equilibrium concentration of vacancies at temperature T.

Force of climb F arises due to two factors

(i) force of attraction between dislocations of opposite nature in the dipole and (ii) line tension of the dislocation.

Force of attraction term = $\dfrac{Gb^2}{2\pi(1-\nu)y}$

Line tension term = $\dfrac{Gb^2}{4\pi(1-\nu)} \dfrac{\ell n(h/b)}{} \dfrac{(dy^2/dx^2)}{[1-(dy/dx)^2]^{3/2}}$

Since line tension force opposes the force of attraction and $dy/dx \ll 1$

$$F \cong \frac{B}{y} - C'\left(\frac{d^2y}{dx^2}\right) \tag{3}$$

Where $B = \dfrac{Gb^2}{2\pi(1-\nu)}$, $C' = \dfrac{Gb^2}{4\pi(-\nu)} \ell n \dfrac{h}{b}$

G is the shear modulus of elasticity at the temperature of consideration.

The flux of vacancies at point O is given by Fick's law:

$$J_O = -D_v \left(\frac{\partial C}{\partial x}\right)_O . \tag{4}$$

Where $D_v \sim 1/6\ \nu b^2 \exp(-U_m/kT)$.

"U_m" is the activation energy for the movement of vacancies in the core.

Number of vacancies migrated across O in time dt = $AJ_0 dt$ (5)

"A" being the area of the core.

Number of vacancies migrated across O in time dt is also equal to $\Delta As'/b^2$, where $\Delta As'$ is the area of the shaded region in Fig. 2.

$$\Delta As' = da/P \tag{6}$$

So we have

$$A\ J_0\ dt = da/Pb^2 \tag{7}$$

Now from Eq. (2)

$$\left(\frac{\partial C}{\partial x}\right)_0 = C_0\, b^2 \exp\frac{Fb^2}{RT} \left(\frac{\partial F}{\partial x}\right)_0 \tag{8}$$

'0' refers to point O in Fig. 2.

$$\left(\frac{\partial F}{\partial x}\right)_0 = -\frac{B}{y^2}\left(\frac{\partial y}{\partial x}\right)_0 - C'\left(\frac{\partial^3 y}{\partial x^3}\right)_0 \tag{9}$$

$$\frac{\partial y}{\partial x} = a\,P\cos px, \qquad \frac{\partial^3 y}{\partial x^3} = -a\,P^3\cos px$$

$$\left(\frac{\partial F}{\partial x}\right)_0 = -B/h^2\ a\,P + C'\ a\,P^3$$

$$\left(\frac{\partial F}{\partial x}\right)_{av.} = 1/2\left[\frac{-B}{h^2}\ a\,P + C'\ a\,P^3\right] \tag{10}$$

From (4), (7), (8) and (10)

$$\frac{da}{dt} = A\ a\ P^2\ b^2\left[\frac{B}{h^2} - C'\,P^2\right]\ \frac{b^2 D}{2kT}\ Co \exp\frac{F_0\, b^2}{kT} \tag{11}$$

On substituting for D and Co, we have

$$\frac{da}{dt} = \frac{A\, a\, P^2\, b^6\, \nu n_0}{12\, kT} \left[\frac{B}{h^2} - C'\, P^2\right] \exp - \frac{U_f + U_m - F_0 b^2}{kT} \tag{12}$$

'n_0' is the number of atoms per unit volume at the core.

Now integrating Eq. (12) from a_1 to a_2 in time t, we have

$$\ell n \frac{a_1}{a_2} = \frac{A\, P^2\, b^6\, \nu n_0\, t}{12\, kT} \left[\frac{B}{h^2} - C'\, P^2\right] \exp - \frac{U_f + U_m - F_0\, b^2}{kT} \tag{13}$$

B. Prismatic Dislocation Loop Connected to the Foil Surfaces by Another Screw Dislocation

Referring to Fig. 3, ΔC, the difference in concentration of vacancies at point 1 and 2 can be written

$$\Delta C = C_{V_0} \left(e^{\mu/kT} - 1\right) \tag{14}$$

Where C_{V_0} is the equilibrium concentration of vacancies at temperature T and μ' is the reduced chemical potential of the vacancy due to the line tension of the dislocation.

From Fick's first law the flux of vacancies along the connecting dislocation, which acts as a pipe is:

$$\text{Flux (number/sec)} = \frac{2AD_V}{S} C_{V_0} \left(e^{\mu/kT} - 1\right) \tag{15}$$

A, is in the area of cross section of the dislocation pipe. D_V is the coefficient of diffusion of vacancies. Let's define N_{V_0} as the fraction of the equilibrium concentration of vacancies

$$N_{V_0} = \frac{C_{V_0}}{1/\Omega}$$

Where Ω is the volume of single vacancy.

Therefore:

$$\text{Flux (number/sec)} = \frac{2A\, D_{V_0}\, N_{V_0}}{S\, \Omega} \left(e^{\mu/kT} - 1\right) \tag{16}$$

The free energy (G^{γ}) of the dislocation loop can be written

$$G^{\gamma} = 2\pi r \Gamma \tag{17}$$

Where Γ is the line tension and r the radius of the loop. The number of vacancies (n_V) in the loop is:

$$n_V = \frac{\pi r^2}{\Omega_s} \tag{18}$$

Ω_s is the area of cross section of one vacancy Eq. 17 can be rewritten as

$$G^{\gamma} = 2\pi r \frac{Gb^2}{4\pi(1-\nu)} \ell n \frac{\alpha r}{r_0} = K\, r\, \ell n \frac{\alpha r}{r_0} \tag{19}$$

r_0 = radius of the core, α = core energy factor, $K = \frac{Gb^2}{2(1-\nu)}$

ν = Poisson's ratio.

Using Equations (17), (18), and (19)

$$\mu = \frac{\partial G^{\gamma}}{\partial r} \frac{\partial r}{\partial n_V} = K \left[1 + \ell n \frac{\alpha r}{r_0}\right] \frac{\Omega_s^2}{2\pi r} \tag{20}$$

Putting this value in Eq. (16)

$$\text{Flux (number/sec)} = \frac{2\, A\, D_{V_0}\, N_{V_0}\, K\, (1+\ell n\, \alpha r/r_0)\, \Omega_s^2}{S\, \Omega^2\, kT\, (2\pi r)} \tag{21}$$

$$e^{\mu/kT} - 1 \cong \frac{\mu}{kT} \quad \text{for} \quad \frac{\mu}{kT} \ll 1.$$

From Eq. (18)

$$\frac{dn_V}{dt} = \frac{2\pi r}{\Omega_s} \frac{dr}{dt} = \text{Flux (number/sec)}$$

and from Eq. (21)

$$\frac{dr}{dt} = \frac{2\,A\,D_P\,K\,(1 + \ell n\ \alpha r/r_0)(\Omega_s)^2}{S\Omega\quad kT\quad (2\pi r)^2} \tag{22}$$

N_{V_0} = D_P = Pipe diffusion coefficient

Equation (22) can be written as:

$$\frac{r^2\,dr}{1+\ell n\ \alpha r/r_0} = C\ \ dt \tag{23}$$

Where

$$C = \frac{3d\ Dp\quad KA}{16\pi\ kTS}\ ,\quad \frac{\Omega_s^{\,2}}{\Omega} = \frac{\pi^2\ d^4 \times 8}{16 \times 4/3\ \pi d^3}$$

$$= \frac{3\pi d}{8}$$

'd' is the diameter of the atom.

Numerically integrating Eq. (23) from r_1 to r_2 in time t, we can find C, hence D_p.

By studying the kinetics at different temperatures, we can determine the equation

$$D_P = D_0\ e^{-\,Eact/kT}$$

'Eact' is the activation energy for the pipe diffusion process.

IV. RESULTS AND DISCUSSION

A. Breaking of Dipoles

Referring to Eq. (12) da/dt is positive when $B/h^2 > C'P^2$, which is the condition for instability to break up. When this condition is satisfied, there is a net flux of vacancies or interstitials away from a (Fig. 4).

In the second case, when $B/h^2 = C'P^2$, there will be no break-up. The dipole shows very little change after a very long time of annealing. This is the condition for the formation of dipoles with dumbell shaped ends except where there is cross over (example for cross over, Fig. 16 dipole F). In the third case, when $B/h^2 > C'P^2$, the dipole opens up due to net flux of vacancies from end toward a. Usually it has been observed that the second condition changes either to the third one, or to the first one.

Since the value of $B = 1.745 \times 10^{-4}$ dynes and value of $C' = 3.52 \times 10^{-4}$ dynes, to satisfy the condition for break up.

$$B/h^2 > C' P^2$$

$$\lambda \geq 2\sqrt{2\pi}\, h$$

Usually for small values of h, this condition for break up can be satisfied either by nonuniform spacing along the dipole or by the end effect.

Nonuniform spacing can lead to breakings anywhere along the dipole for example in Fig. 8 (A, B) and in Fig. 9 I, II, at A.

The end effect, which is more common is due to the fact that at the end b (Fig. 4), the chemical C'/σ is always more than B/h at point a,

because $\sigma \leq h/2$. So there is a net flux of vacancies or interstitials from b to a. As a result of this net flux, the dipole tries to open at the end and this may lead to a fluctuation where $B/h^2 > C'P^2$. When this condition is satisfied, there is net flux of vacancies or interstitials away from a (Fig. 4), which leads to breaking up of the dipole (example Fig. 8 I and II at C.)

However, if h is sufficiently large to start with, the fluctuation would lead either to $B/h^2 = C'P^2$ or $B/h^2 < C'P^2$. In that case, the dipole will either remain stable with dumbell shaped ends, for example, Fig. 17 dipole A or open up Fig. 16 dipole G or Fig. 17 dipole C.

The argument, given by Groves and Kelly,[6] for breaking at the end is that since $C/\sigma > B/h$ at the end, the two sides will move away from one another providing the first step in the formation of a circular loop or in the break up. But as we have proved, this is not a sufficient condition for breaking up, it may lead to any one of the three situations mentioned above.

Once this instability is set up, a further difference in chemical potentials is created between c and d (Fig. 4) which leads to instability and break up. Thus there is a wavelike pattern set up, starting from both ends. Its wavelength increases and the amplitude gets damped as the difference in chemical potentials between successive points (c and d, e and f) goes on decreasing, for example, Fig. 8 I and II dipoles D and E.

Taking $A = 10\ b^2$, $\nu = 10^{13}$, $n_0 = 1/b^3$ and measuring experimentally $\lambda = 1660\ A^\circ$, $(a_2/a_1)_{av} = 1.15$, $h = 167\ A^\circ$ from Figs. 11 and 12 at A and B. From Fig. 8 at B $(a_2/a_1)_{av} = 1.2$, $h = 170$ A, Eq. (13) gives $U_f + U_m = 60,700 \pm 2,000$ cal/mole.

Figure 10 shows the dipoles after less annealing time.

Within the experimental accuracy of measurements the value of the activation energy obtained for pipe diffusion from breaking in the middle as well as breaking at the ends is the same. However as it was pointed out previously, the theory is very good only for the breaking in the middle, where the total diffusion path of ions does not exceed the wavelength of the fluctuation. This is particularly true at the intial stages.

B. Connected Dislocation Loop and Comparison

The diffusion equation, obtained using this approach is

$$D_p = 1.5 \times 10^{-3} \exp\left(\frac{-60,400}{RT}\right)$$

and the value of entropy $\Delta S = 0.1$ cal/mole·deg assuming $D_p = 1/6\ \nu b^2 \exp(-Eact/RT)$, using Figs. 13, 14, 15 and Table I.

The remarkable agreement between the two theories not only proves that proposed models are sound, but also that the same diffusion process (pipe diffusion) is involved in both cases. Further it is to be noted annealing temperature in the dipole breaking experiment is only 1200°K, but the activation energy is the same. This shows that the kinetics of pipe diffusion can be described by a diffusion equation similar to that of bulk diffusion.

The upper limit of the activation energy 71,300 ± 4600 cal/mole, estimated by Groves and Kelly[6] also seems reasonable. However, their upper limit is not very accurate, as the value of h (separation between the dipoles) was a matter of guess. Also since the separation of dipoles is pretty inhomogeneous, using the total time for breaking to estimate

the upper limit of activation energy does not carry any meaning.

In the diffusion process, both oxygen and magnesium ions take part. However, the rate is controlled by oxygen ion mobility as this is the slower moving species.[8,9]

The fact that the diffusion process is controlled by oxygen ion mobility can be further checked as follows. Assuming no leakage from the dislocation pipe, during the pipe diffusion process and cylindrical diffusion during bulk diffusion, the last is especially true for thin foils.

Then at least for the equal rate of shrinkage of the dislocation loop during bulk and pipe diffusion, we should have:

$$D_P \times \text{areas of the pipe} = D_b \times \text{area of the dislocation loop}$$

$$D_P \times 10\, b^2 = D_b \times 60{,}000\, b^2$$

$$D_P \cong (10^3 - 10^4)\, Db.$$

Using the above value of D_P and taking D_b from Refs. 8 and 9 we find:

$$\frac{D_P}{D_b \text{ (for oxygen)}} \cong 10^3 \; e^{\frac{2{,}000}{RT}} \cong 10^3$$

$$\frac{D_P}{D_b \text{(for magnesium)}} \cong 10^{-2} \; e^{\frac{18{,}600}{RT}} \cong 1$$

Figure 16 is an example which shows that the shrinkage rate in the pipe diffusion process is a little higher than that in the bulk diffusion process. Under similar conditions after 1 hour and 21 minutes loops A and B have disappeared in V by the pipe diffusion process, where as there is a comparatively small change in C, D and E, which are shrinking by the bulk diffusion process. This conclusion is based primarily on

A as B is very close to the surface. As we showed, agreement is good for the assumption of equal rates. These discrepancies may be attributed to surface conditions of the foil. The foil for pictures in Figs. 13, 14 and 15 is different from that for pictures in Fig. 16. Also theory assumes that the atoms after coming at the surface go to equilibrium sites (i.e. ledges at the surfaces) and thus neglects rearrangement energy. This arrangement not only depends upon surface conditions but also upon the cleanliness around the opening of the connecting dislocation at the surface.

Groves and Kelly[6] were very happy to find their upper limit for activation energy between activation energy for the bulk diffusion of magnesium in MgO 3.4 ± 0.1 eV[8] and that for diffusion of oxygen in MgO 2.7 ± 0.3 eV.[9] Apparently they thought the process is controlled by both oxygen and magnesium ion mobilities because then:

$$E_{act(\text{for pipe diffusion})} \cong 1/2\ E_{act(\text{for bulk diffusion})}$$

$$\cong 1/2[\Delta Hm_{Mg^{++}} + \Delta Hm_{O^{--}} + E_{f\ Mg^{++}} + E_{f\ O^{--}}]$$

$\Delta Hm_{Mg^{++}}$ = Activation energy of migration for Mg^{++}

$E_{f\ Mg^{++}}$ = Energy of formation of cation vacancy

$\Delta Hm_{O^{--}}$ = Activation energy of migration for O^{--}

$E_{f\ O^{--}}$ = Energy of formation of anion vacancy

However, as we have shown, it should be

$$E_{act(\text{for pipe diffusion})} \cong 1/2[\Delta Hm_{O^{--}}\ E_{f\ Mg^{++}} + E_{f\ O^{--}}]$$

It assumes that the diffusion process involves Schottley defects, which is reasonable in view of the size difference between anion and cation.

The very small positive value of entropy is also understood, as only a very small fraction of the total number of atoms take part in the diffusion process and the process is limited within the pipe itself.

V. CONCLUSIONS

When dipoles, introduced by plastic deformation in magnesium oxide are annealed they break up into rows of prismatic loops by the pipe diffusion process.

The equation for the pipe diffusion is

$$D_P = 1.5 \times 10^{-3} \exp\left(\frac{-60,400}{RT}\right)$$

The diffusion process is controlled by oxygen ion mobility.

ACKNOWLEDGMENTS

The author is grateful to Professor Jack Washburn for his guidance and encouragement throughout this investigation. My special thanks are also due to Professor J. E. Dorn for helpful discussions in developing the two models.

This was done under the auspices of the U. S. Atomic Energy Commission through the Inorganic Materials Research Division of the Lawrence Radiation Laboratory.

REFERENCES

1. J. Washburn, G. W. Groves, A. Kelly and G. K. Williamson, Phil. Mag. 5, 991 (1960).

2. G. W. Groves and A. Kelly, Proc. Roy. Soc. 275A, 233 (1963).

3. J. Washburn, Electron Microscopy and Strength of Crystals, Chapt. 6, Editors, G. Thomas and J. Washburn, Interscience, N. Y. (1963).

4. T. R. Cass, Ph. D. Thesis, University of California, Berkeley (1965).

5. A. S. Teleman, Acta Met. 10, 813 (1962).

6. G. W. Groves and A. Kelly, J. Appl. Phys. 33, 456 (1962).

7. G. W. Groves and A. Kelly, J. Appl. Phys. 34, 3104 (1963).

8. R. Linder and G. D. Parfitt, J. Chem. Phys. 26, 182 (1957).

9. Y. Oishi and W. D. Kingery, J. Chem. Phys. 33, 905 (1960).

10. J. Narayan and J. Washburn, to be published.

TABLE 1.

Sample No.	Radius in A
B_1	1500
B_2	1500
B_3	700
B_4	595
B_5	573
B_6	539
B_7	438

Temperature	Dv (cm^2/sec)
1640°K	1.5×10^{-11}
1553°K	5.1×10^{-12}
1440°K	1.05×10^{-12}

Figure Captions

Fig. 1. Slip band structure after plastic deformation (bending) at room temperature. Slip bands appear only on (110), $(1\bar{1}0)$, (101) and $(\bar{1}01)$ planes. N. B. projection of {101} slip bands is along [010] direction.

Fig. 2. Model for dipole breaking.

Fig. 3. Model for pipe diffusion through a screw dislocation connected to both surfaces of the foil from a prismatic dislocation loop inside the foil.

Fig. 4. Mechanism of wave pattern formations in the dipoles during annealing.

Fig. 5. Shear modulus of elasticity of magnesium oxide single crystals versus temperature.

Fig. 6. $r^2/1 + \ell n \frac{\alpha r}{r_o}$ vs r graph taking $\alpha = 2$ and $r_o = 2b$.

Fig. 7. Coefficient of pipe diffusion versus $(\frac{1}{T})$ graph.

Fig. 8. I annealed for 196 min at 1700°F; II same area as I annealing further for 60 min.

Fig. 9. I, II and II show that breaking at A is due to nonuniform dipole spacing.

I after room temperature deformation, foil is annealed at 1700°F for 75 min

II same foil as I, after annealing further at 1700°F for 30 min

III same foil as I, after annealing further at 1700°F for 31 min.

Fig. 10. After deforming at room temperature, foil was annealed for 136 minutes at 1700°F.

Fig. 11. Same area as in Fig. 10 after annealing 30 min. at 1700°F.

Fig. 12. Same area as in Fig. 11 after further annealing 30 min at 1700°F.

Fig. 13. B_1 after room temperature deformation annealed for 40 min at 2491°F.

B_2 same area annealed further for 20 min at 2491°F.

Fig. 14. B_3 same area annealed further for 32 min at 2491°F

B_4 same area annealed further for 10 min at 2491°F

B_5 same area annealed further for 15 min at 2060°F

Fig. 15. B_6 same area as above annealed further for 30 min at 2040°F

B_7 same area as above annealed further for 26 min at 2335°F

B_8 annealed same loop further for 40 min at 2335°F.

Fig. 16. IV After room temperature deformation foil is annealed for 7 hours 28 min at 1700°F plus 135 min at 2335°F.

V same area as IV, annealed further for 1 hour 21 min at 2335°F

Fig. 17. After room temperature deformation foil is annealed for 7 hours 28 min at 1700°F plus 30 min at 2335°F.

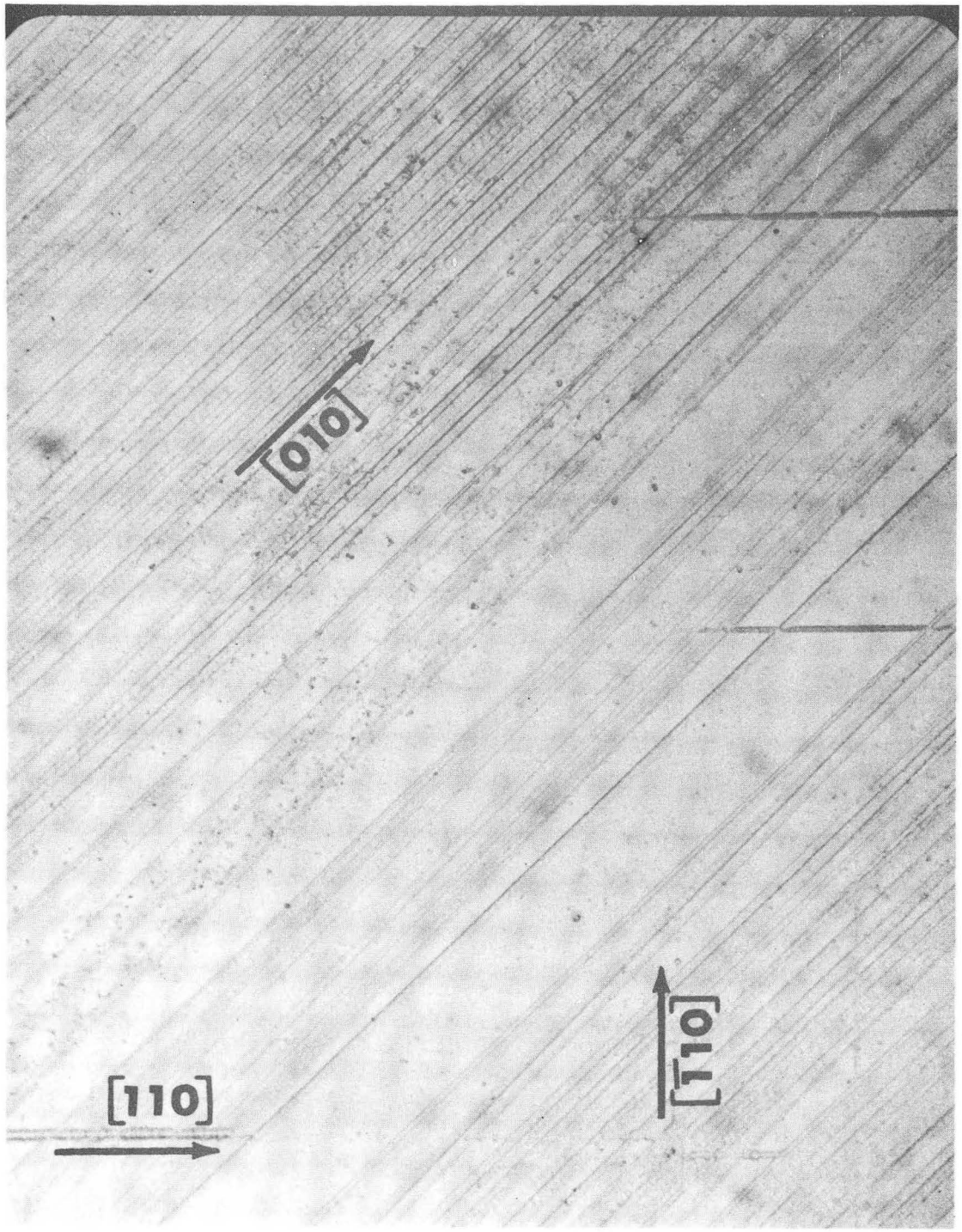

164X XBB 709-3893

Fig. 1

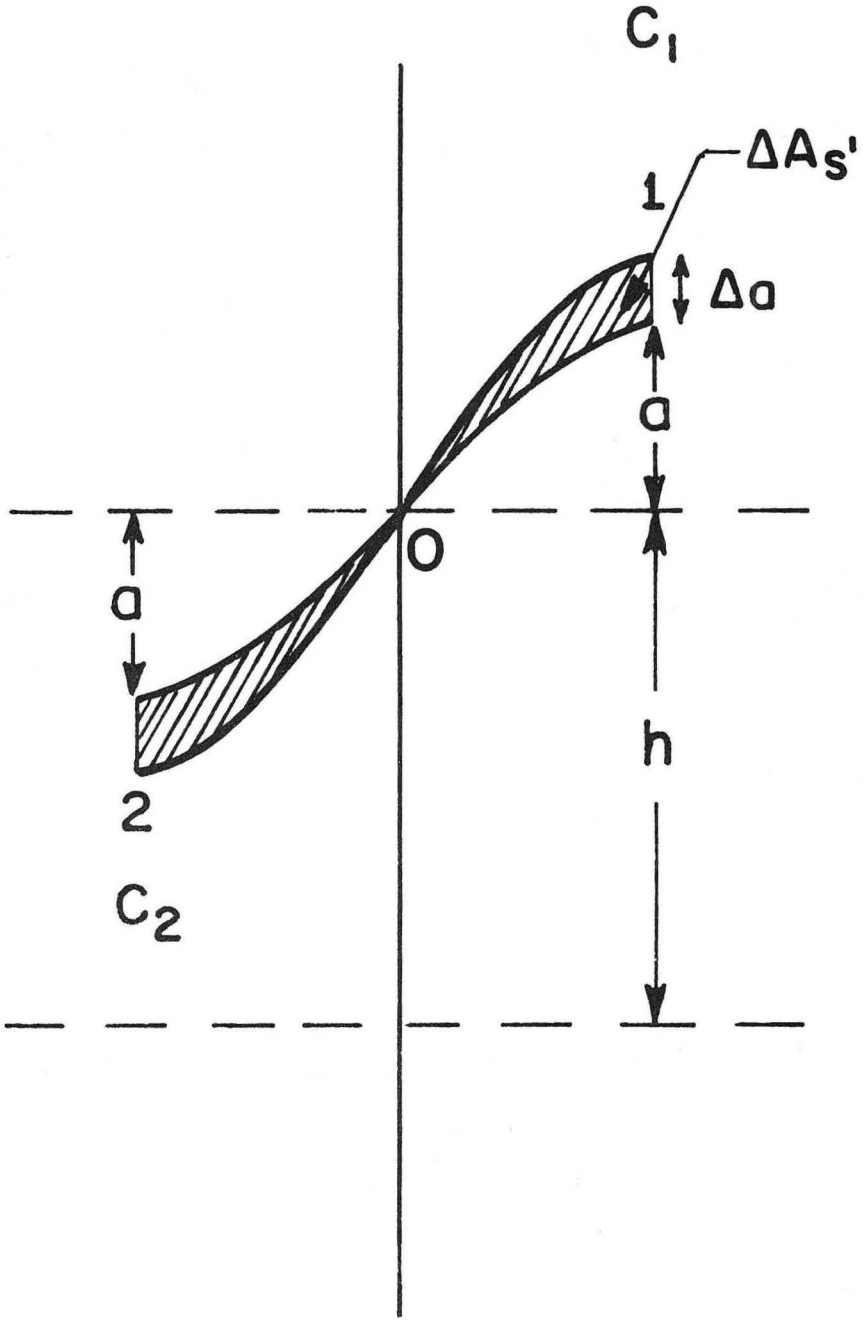

XBL 709-6561

Fig. 2

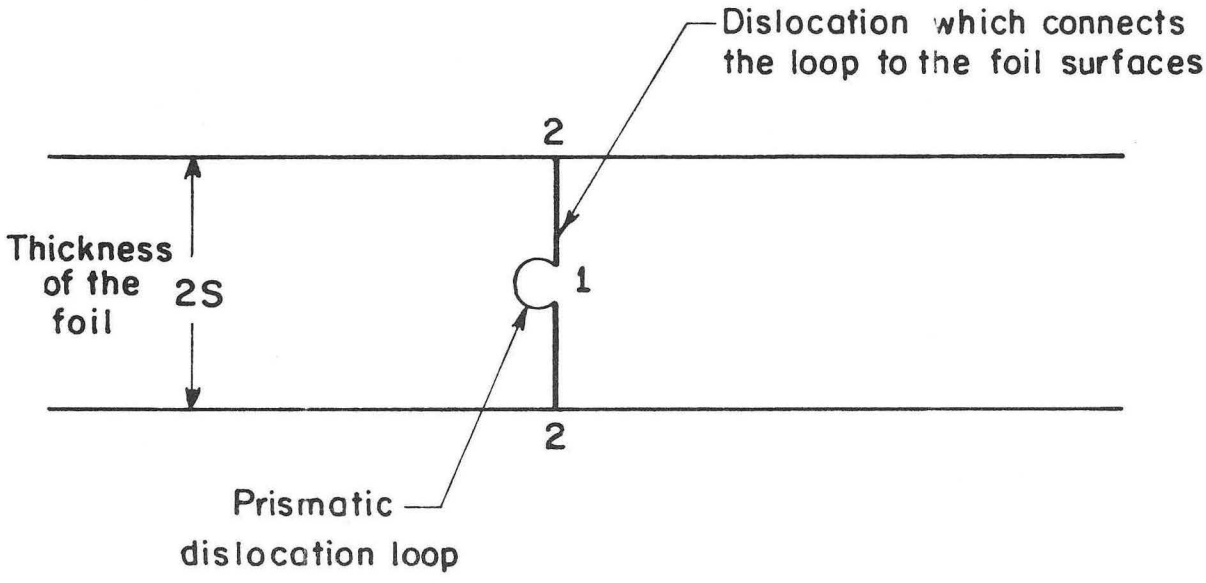

XBL 709-6565

Fig. 3

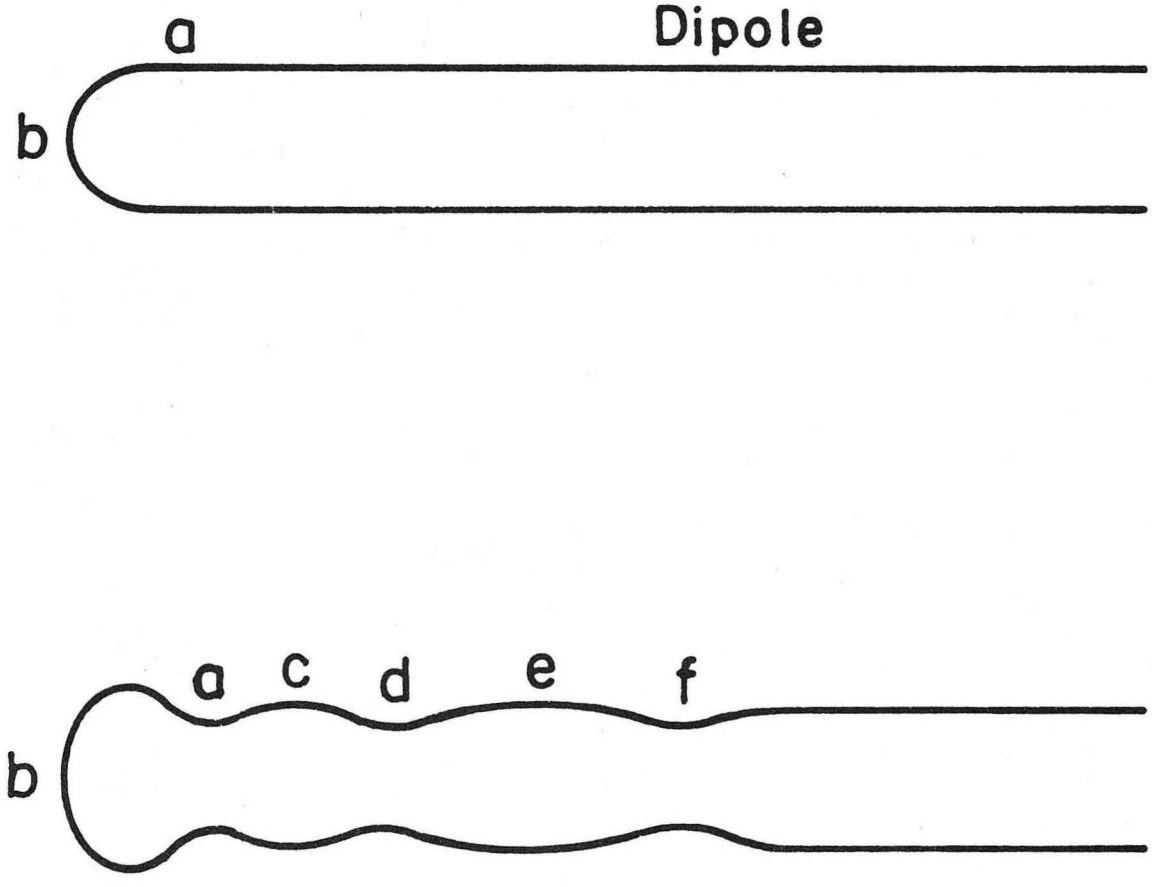

Dipole Breaking

XBL 709-6562

Fig. 4

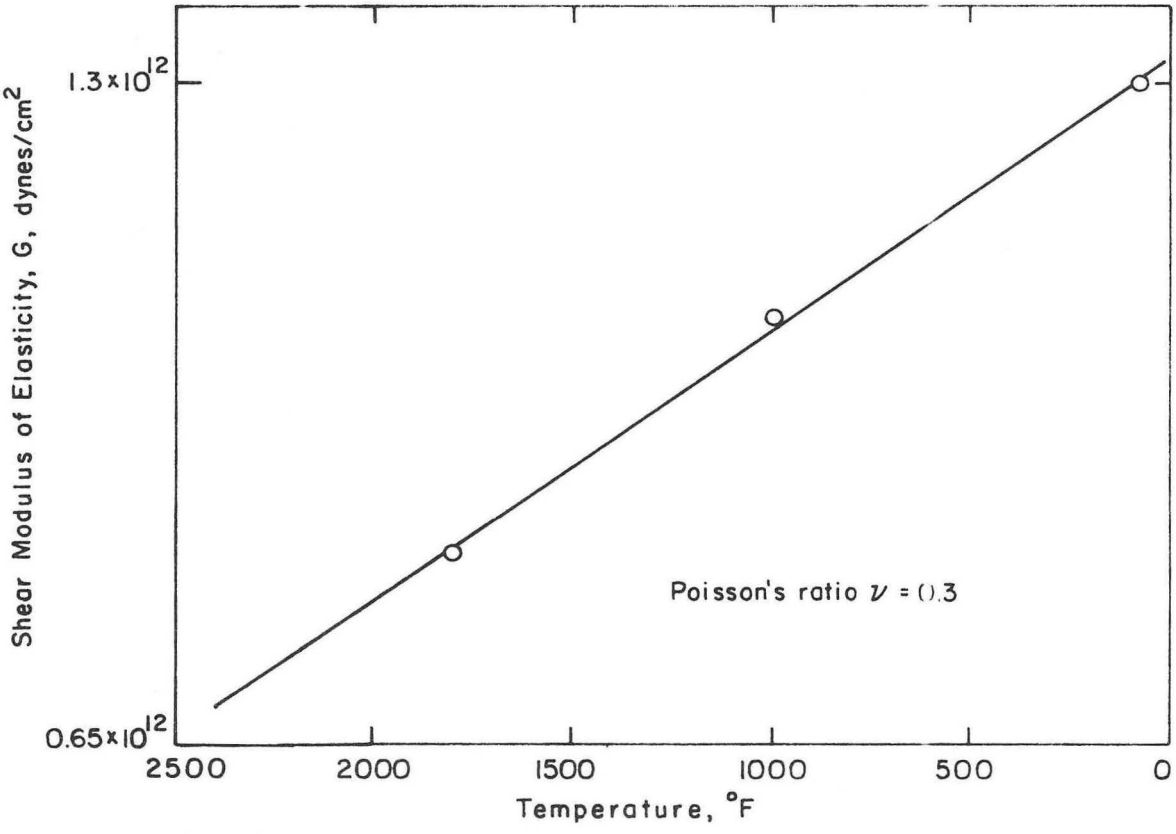

XBL 709-6564

Fig. 5

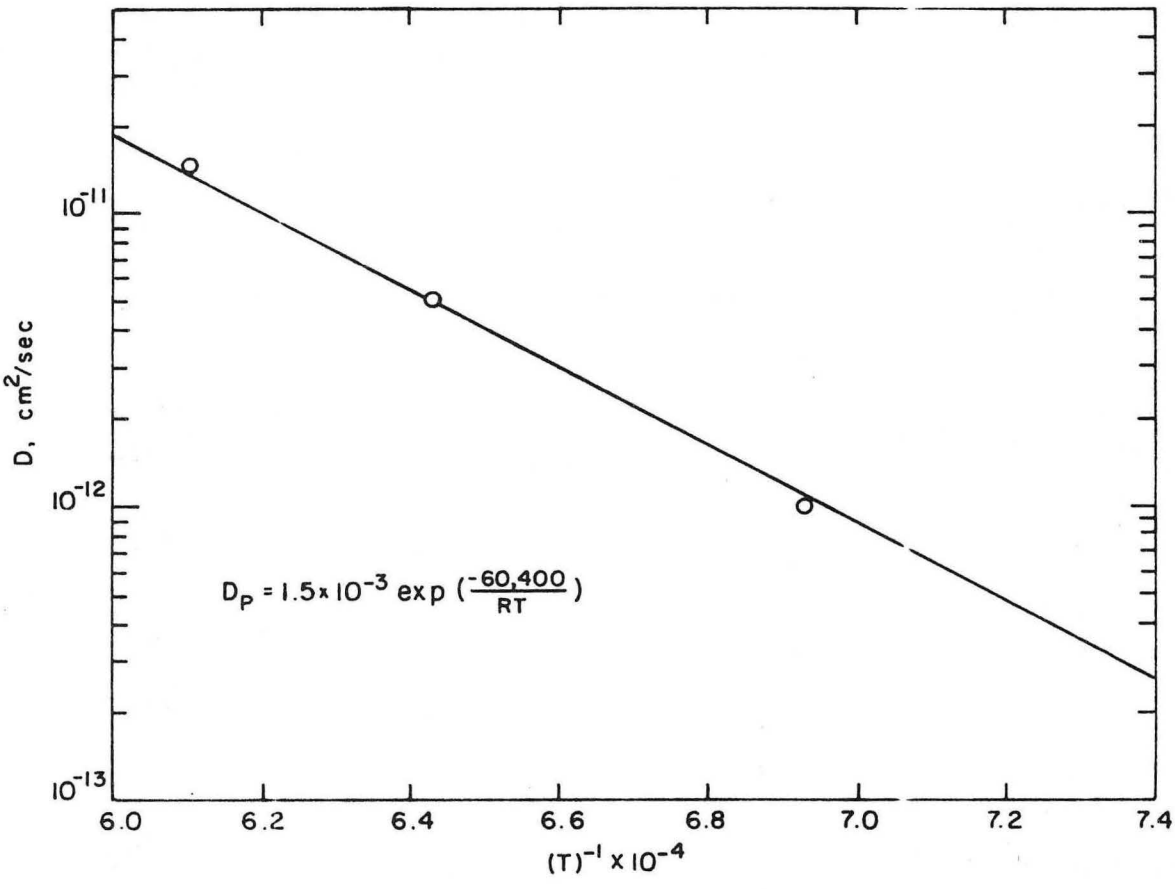

XBL 709-6563

Fig. 6

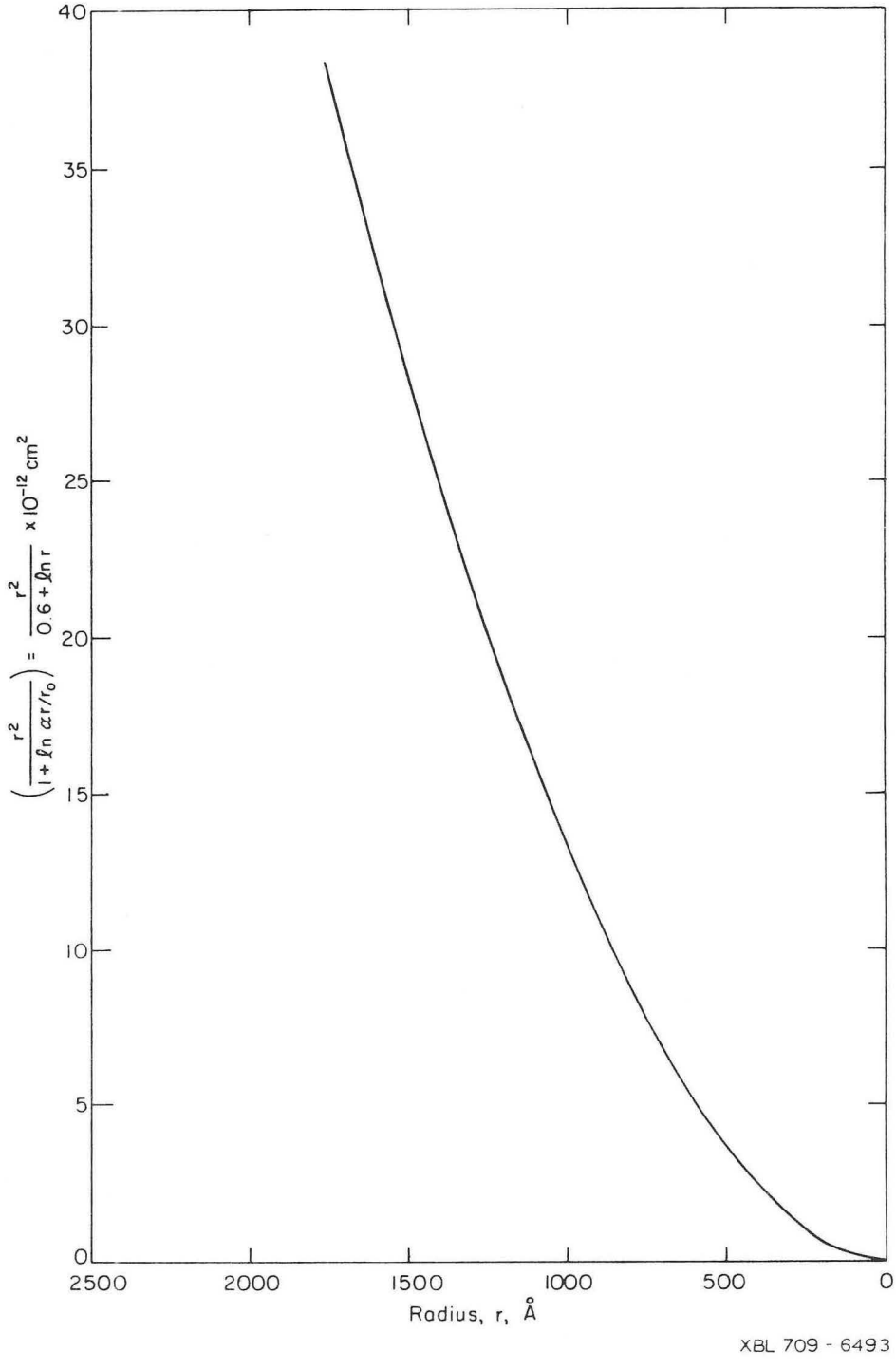
40
35
30
25
20
15
10
5
0
2500
2000
1500
1000
500
0
Radius, r, Å
$\left(\frac{r^2}{1+\ell n\, \alpha r/r_o}\right) = \frac{r^2}{0.6+\ell n\, r} \times 10^{-12}\ cm^2$
XBL 709 - 6493

Fig. 7

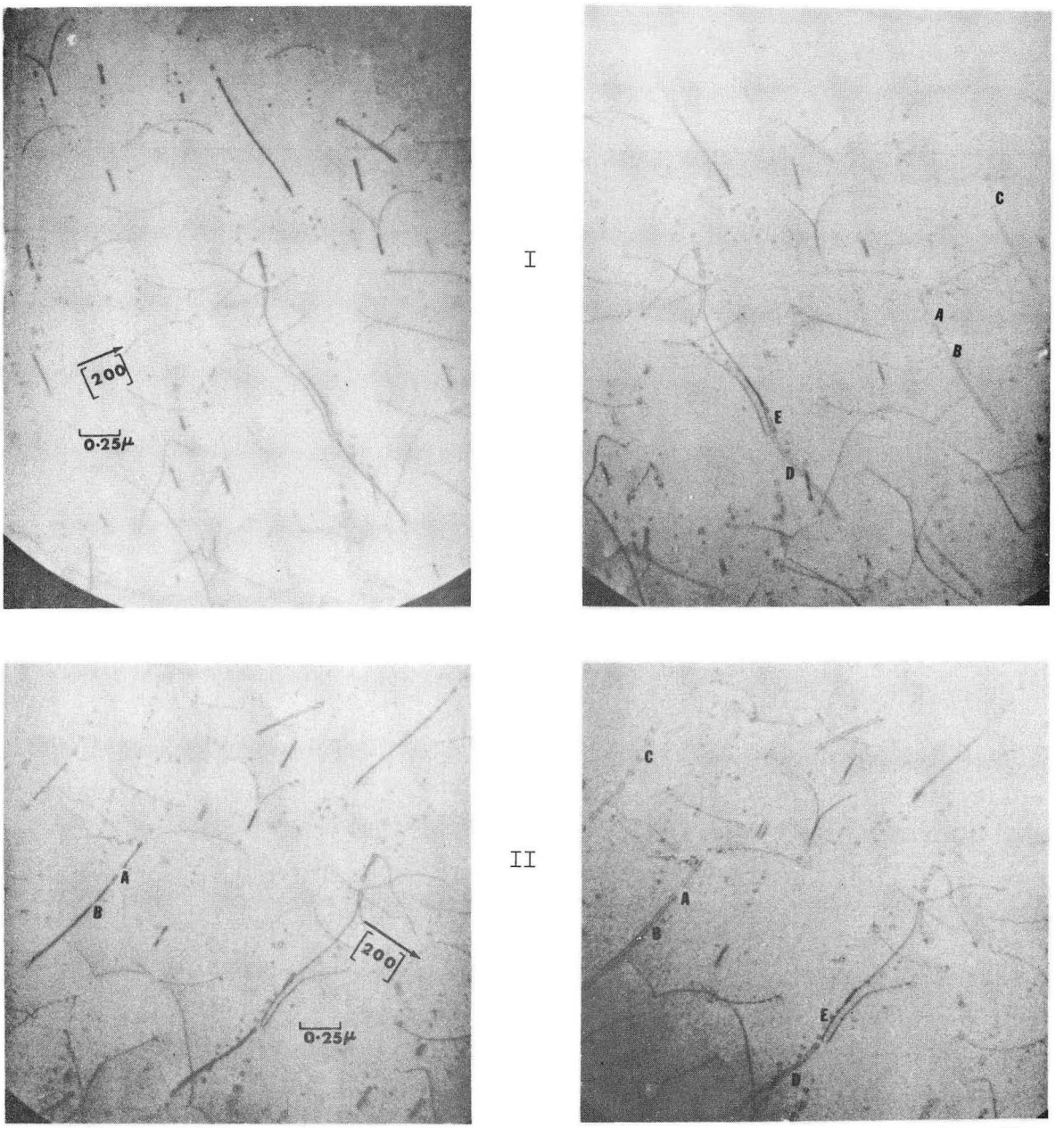

XBB 709-3890

g+ve g-ve

Fig. 8

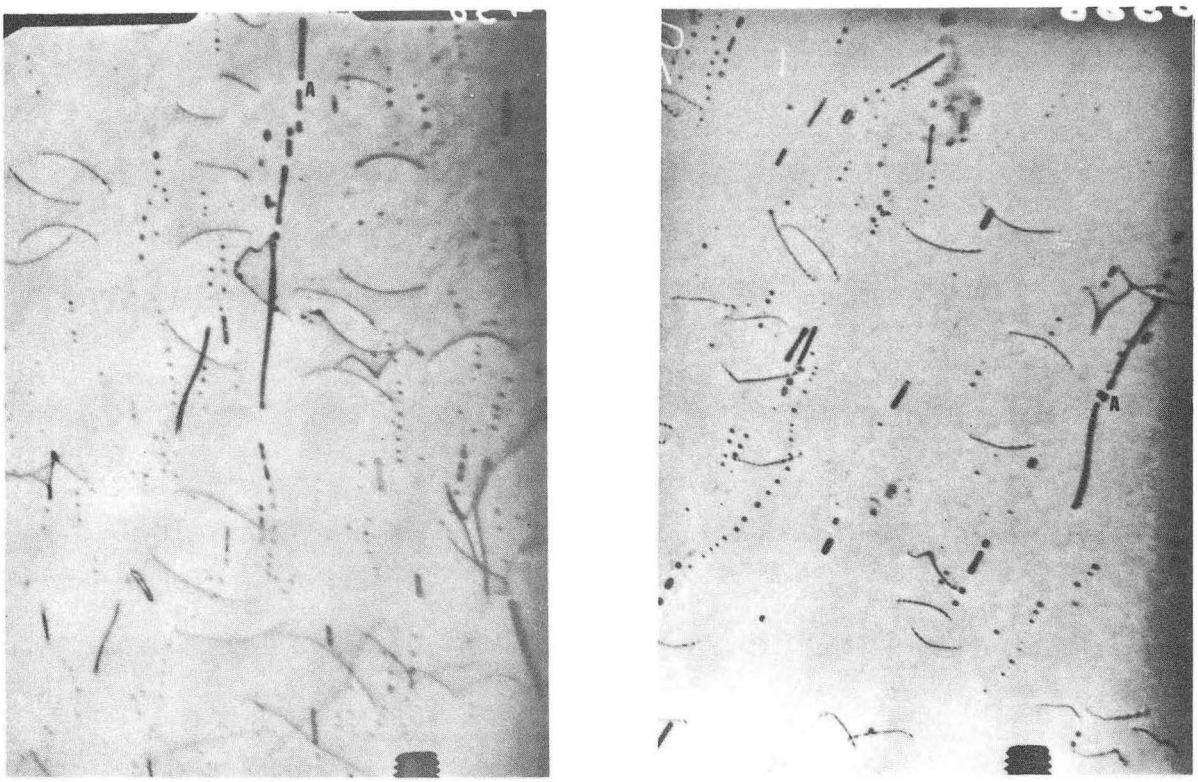

XBB 709-3907

I 24800X II

Fig. 9

XBB 709-3885

22050X

Fig. 10

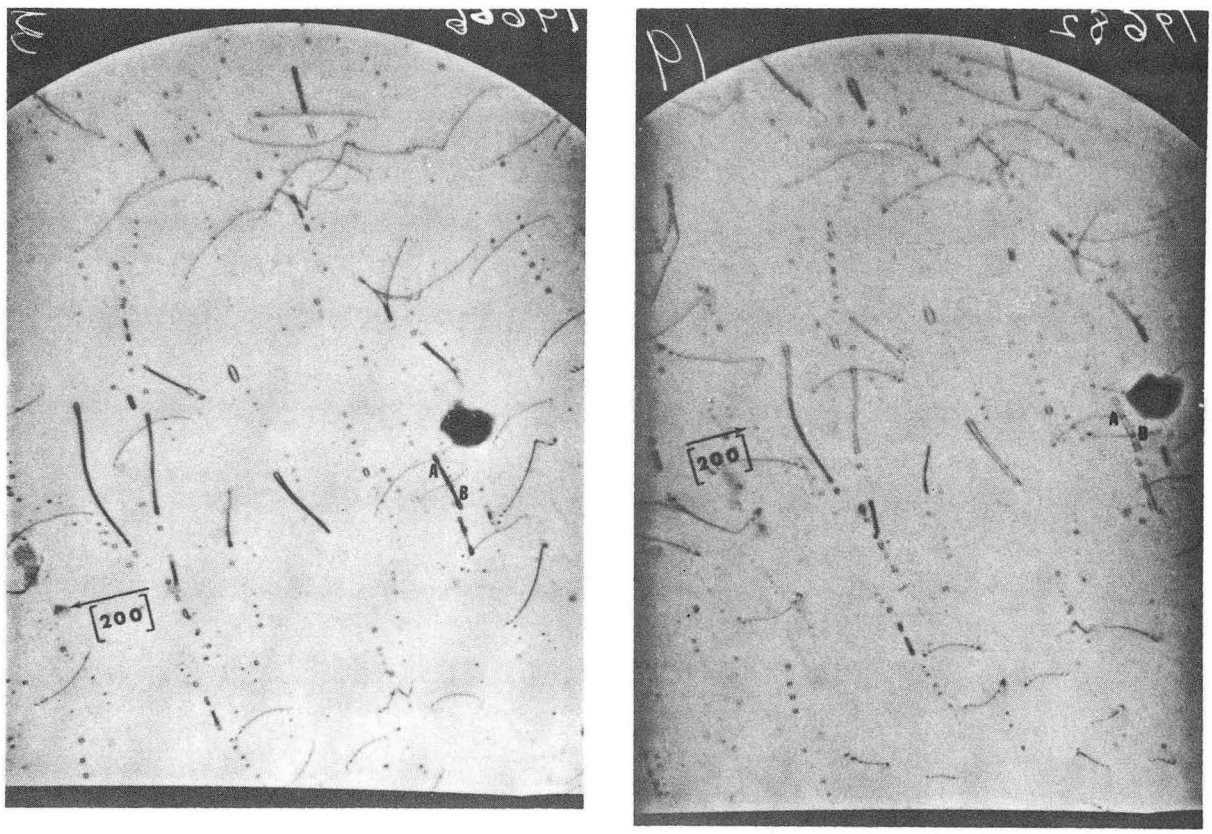

XBB 709-3889

22100X

Fig. 11

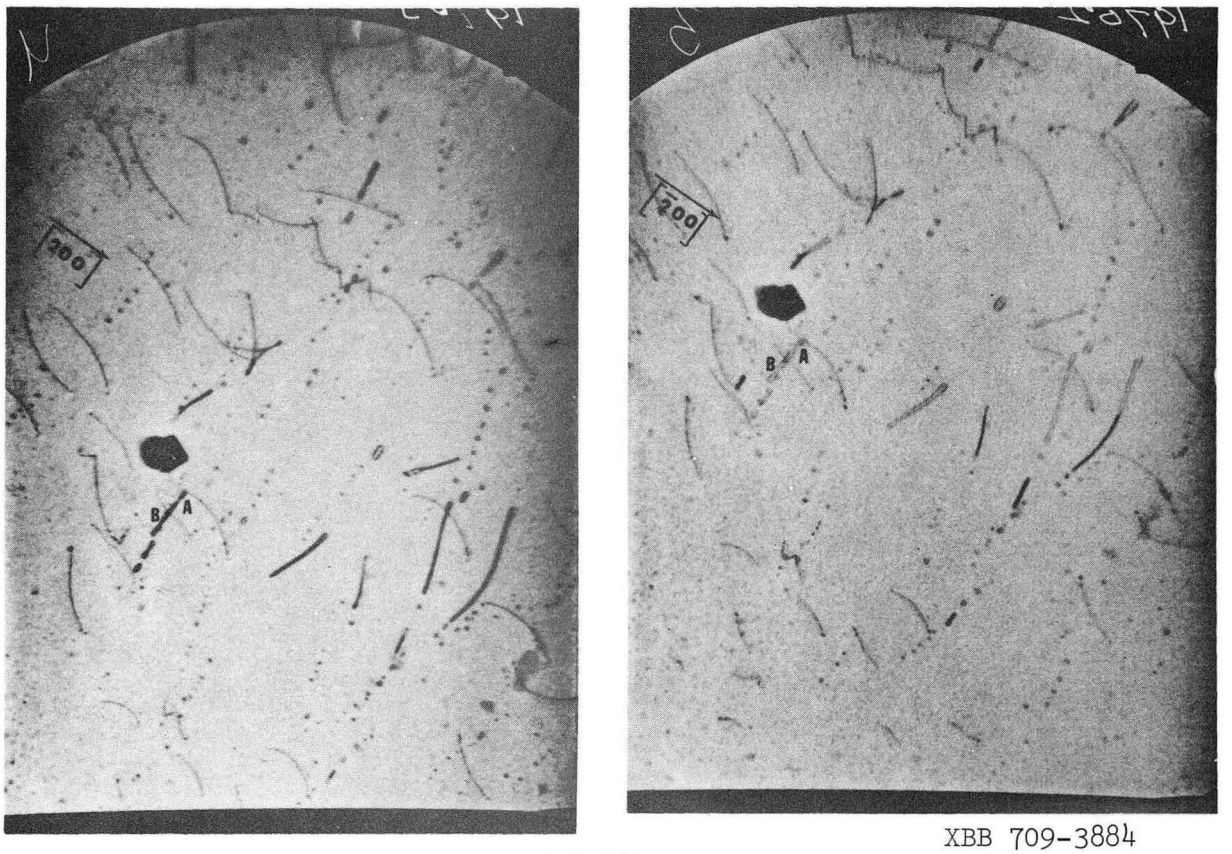

XBB 709-3884

21750X

Fig. 12

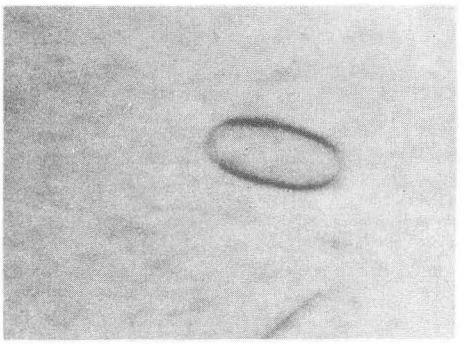

B_1

46350X

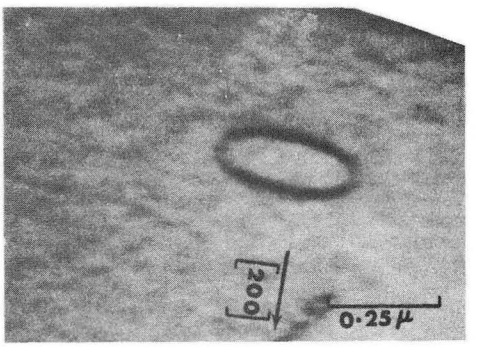

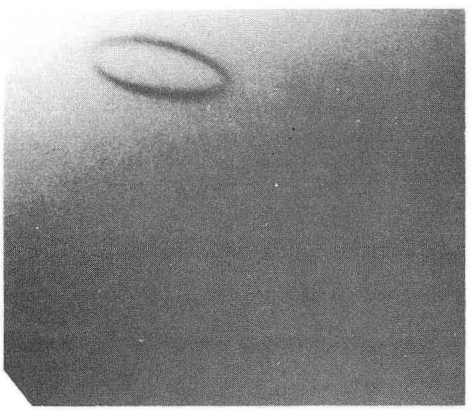

B_2

46350X

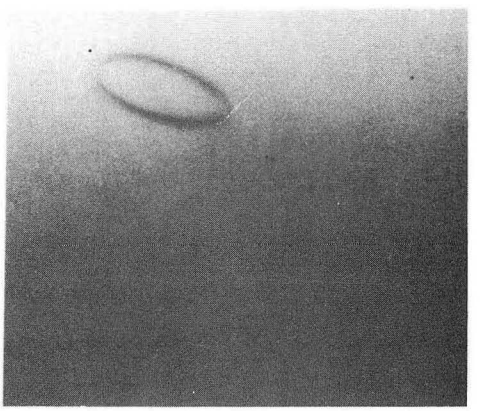

g+ve

g-ve

XBB 709-3896

Fig. 13

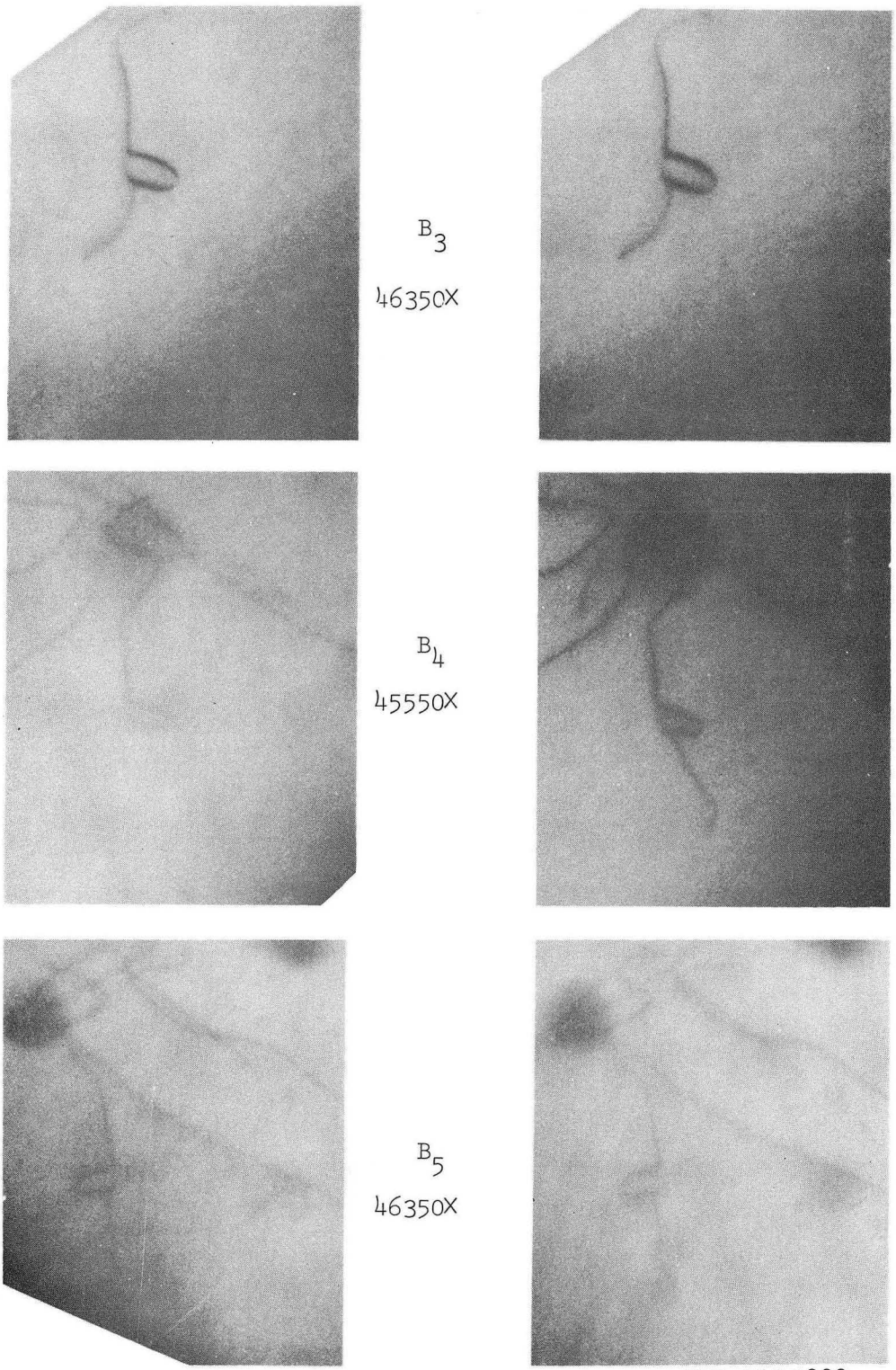

g+ve g-ve

Fig. 14

B_6

46550X

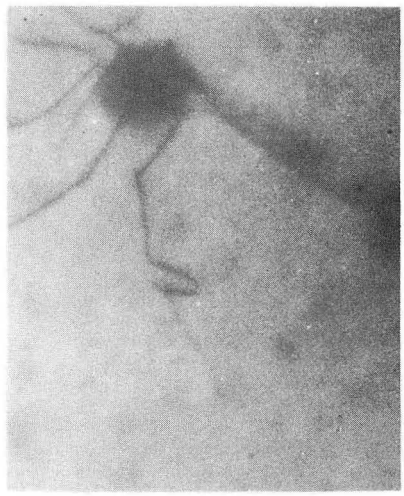

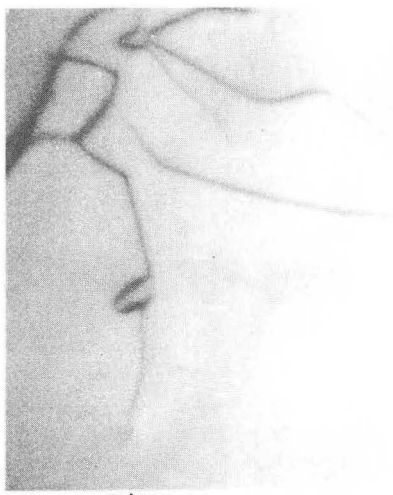

B_7

47500X

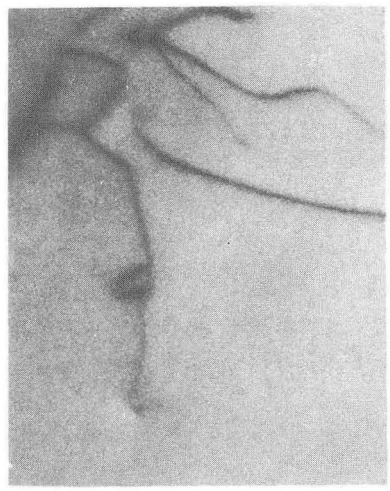

g+ve

g-ve

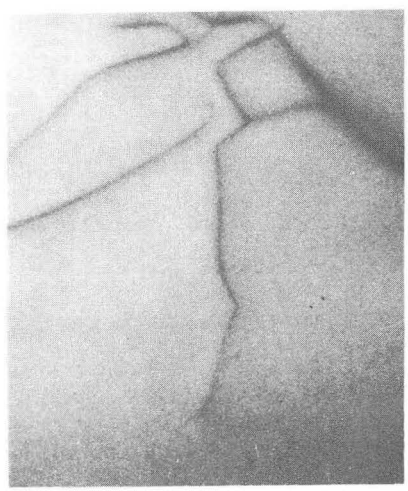

B_8

XBB 709-3887

Fig. 15

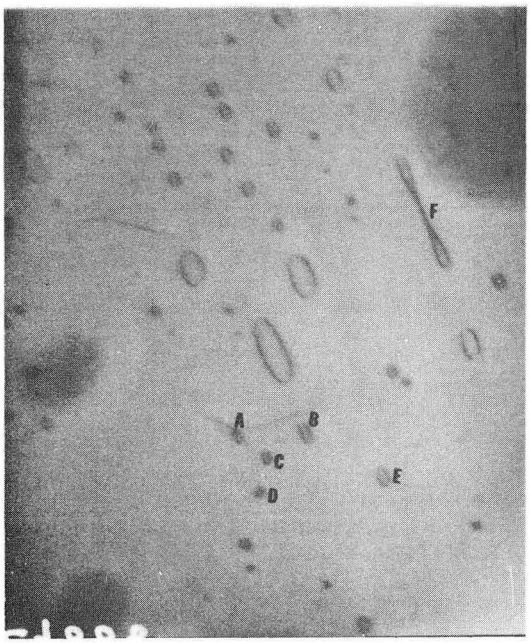

IV

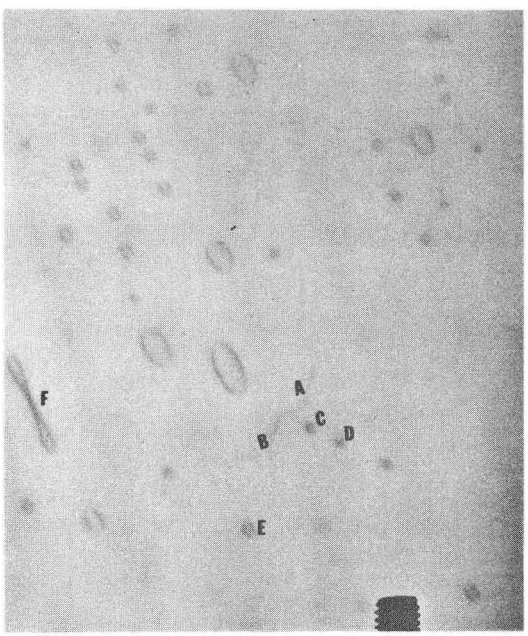

V

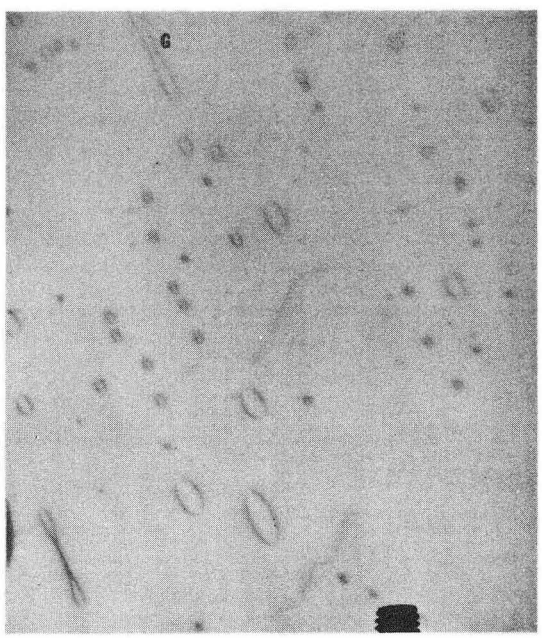

29961X

29905X XBB 709-3886

Fig. 16

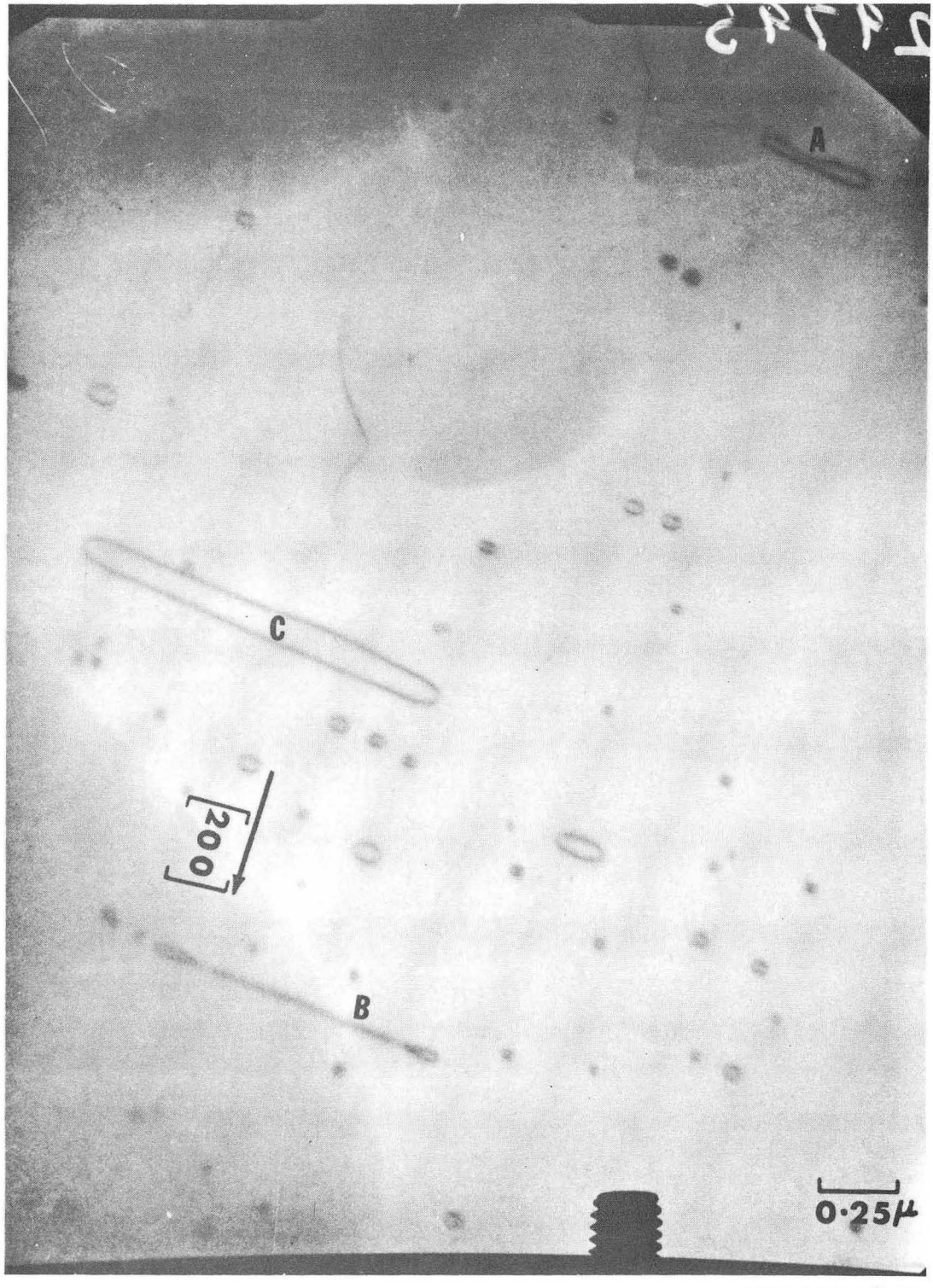

XBB 709-3897

Fig. 17

LEGAL NOTICE

This report was prepared as an account of Government sponsored work. Neither the United States, nor the Commission, nor any person acting on behalf of the Commission:

A. Makes any warranty or representation, expressed or implied, with respect to the accuracy, completeness, or usefulness of the information contained in this report, or that the use of any information, apparatus, method, or process disclosed in this report may not infringe privately owned rights; or

B. Assumes any liabilities with respect to the use of, or for damages resulting from the use of any information, apparatus, method, or process disclosed in this report.

As used in the above, "person acting on behalf of the Commission" includes any employee or contractor of the Commission, or employee of such contractor, to the extent that such employee or contractor of the Commission, or employee of such contractor prepares, disseminates, or provides access to, any information pursuant to his employment or contract with the Commission, or his employment with such contractor.

TECHNICAL INFORMATION DIVISION
LAWRENCE RADIATION LABORATORY
UNIVERSITY OF CALIFORNIA
BERKELEY, CALIFORNIA 94720